☙

Observation of a spin-density wave node on antiferromagnetic Cr(110) islands

Pin-Jui Hsu,[1] Tobias Mauerer,[1] Weida Wu,[2] and Matthias Bode[1,3]

[1]*Physikalisches Institut, Universität Würzburg, 97074 Würzburg, Germany*

[2]*Department of Physics and Astronomy and Rutgers Center for Emergent Materials, Rutgers University, Piscataway, New Jersey 08854, USA*

[3]*Wilhelm Conrad Röntgen-Center for Complex Material Systems (RCCM), Universität Würzburg, Am Hubland, 97074 Würzburg, Germany*

We have performed a detailed study of the evolution of the charge-density wave (CDW) and spin-density wave (SDW) on the surface of nanoscale Cr islands grown on W(110). Using low-temperature scanning tunneling microscopy (STM), we find a striking nonmonotonic thickness dependence of the CDW wavelength at 50 K. As the local island thickness Θ decreases from about 50 to 5.2 nm, the CDW wavelength gradually increases from the bulk value by approximately 30%. We find a gap without any CDW at coverages Θ_{gap} between 5.2 and 3.7 nm. Spin-resolved STM data reveal that within this CDW gap the SDW modulation also disappears on the Cr island surface. At $\Theta < 3.7$ nm the CDW reappears. This unusual behavior of CDW and SDW in Cr nanoislands can be understood by a reorientation of the SDW wave vector **Q** which is potentially driven by the pinning of the SDW node at the island surface at Θ_{gap}.

I. INTRODUCTION

The physics of charge-density (CDWs) and spin-density-waves (SDWs) have drawn much attention regarding their fundamental properties as well as their potential for future applications in technology. Sample systems investigated so far include a wide range of materials, including one-dimensional (1D) atomic chains,[1–3] layered two-dimensional (2D) structures,[4–7] or iron-based superconductors.[8–11] Among structurally more simple systems elemental chromium (Cr) has been regarded as a model system, as it is an itinerant antiferromagnet and exhibits both, CDW and SDW phenomena which appear to be closely correlated.[4,12] Moreover, the important role of the SDW on the giant magnetoresistance effect of Cr has been demonstrated,[13,14] with significant implications for spintronic devices.

Scanning tunneling microscopy (STM) investigations of Cr(110) surfaces were first performed on monocrystal samples. In fact, the surface projections of CDW domains were visualized by Braun *et al.*[15] They found three different domains corresponding to the three possible orientations of the CDW wave vector **Q** along any of the three ⟨100⟩ directions of the bcc lattice. Later on, spin-polarized STM (SP-STM) was used to investigate the spin structure of Cr(110) thin films on W(110) in real space.[16] While the incommensurate SDW was confirmed for relatively thick films [≈100 atomic layers (ALs)], a long-range modulation of the antiferromagnetic spin structure with a wavelength of 7.7 ± 0.5 nm along the [001] direction was found at monolayer (ML) Cr coverage.

These examples indicate that by reducing the dimensionality from bulk to thin film, a rich variety of CDW properties associated with the incommensurate SDW behavior can be expected for antiferromagnetic (AFM) Cr islands. However, there are very few studies on the magnetic properties of nanoscale AFM islands in the literature. Herein we present a systematic STM study of the thickness and temperature dependence of the CDW and SDW of nanoscale Cr islands on W(110). The moiré pattern and the thickness-dependent distribution of the CDW are observed by STM. Our data reveal an intriguing CDW gap around 4.5 nm Cr thickness where the CDW modulation is absent. By utilizing the SP-STM technique with both in-plane and out-of-plane sensitive probe tips, the spin structure is mapped out for local coverages within and outside the CDW gap. These data suggest that the Cr surface is nonmagnetic in the CDW gap region.

II. EXPERIMENTAL SETUP AND PROCEDURES

The experiments were performed in an ultrahigh vacuum (UHV) multifunctional chamber with the base pressure $p < 1 \times 10^{-10}$ mbar. The clean W(110) substrate was prepared by cycles of oxygen annealing and flashing up to 2300 K.[17] Cr was deposited onto the substrate at room temperature at a deposition rate of about 1 atomic layer (AL) per minute as calibrated by STM. Upon deposition the sample was postannealed at temperatures ranging from 600 to 800 K. Similar to earlier results on Fe/W(110), higher annealing temperature resulted in Cr islands with smaller lateral size but higher thickness.[18,19] The crystalline structure was characterized by low-energy electron diffraction (LEED). For spin-polarized (SP)-STM measurements[20–22] the sample was transferred into a variable-temperature (VT) scanning tunneling microscope. By adjusting the flow of liquid helium through a continuous-flow cryostat, it allows for measurements at sample temperatures down to 35 K. Spin-sensitive measurements were performed with magnetic probe tips. In-plane[23–25] and out-of-plane[26–28] sensitivity was achieved by Fe-coated W tips and Ni bulk tips, respectively. The magnetization direction of magnetic probe tips was experimentally confirmed by reference measurements on the spin spiral of monolayer Mn films on W(110).[29–31]

III. RESULTS AND DISCUSSION

Figure 1(a) shows the STM morphology of three Cr islands on a stepped W(110) substrate. The islands were grown by depositing an average Cr coverage of 12 AL and postannealing
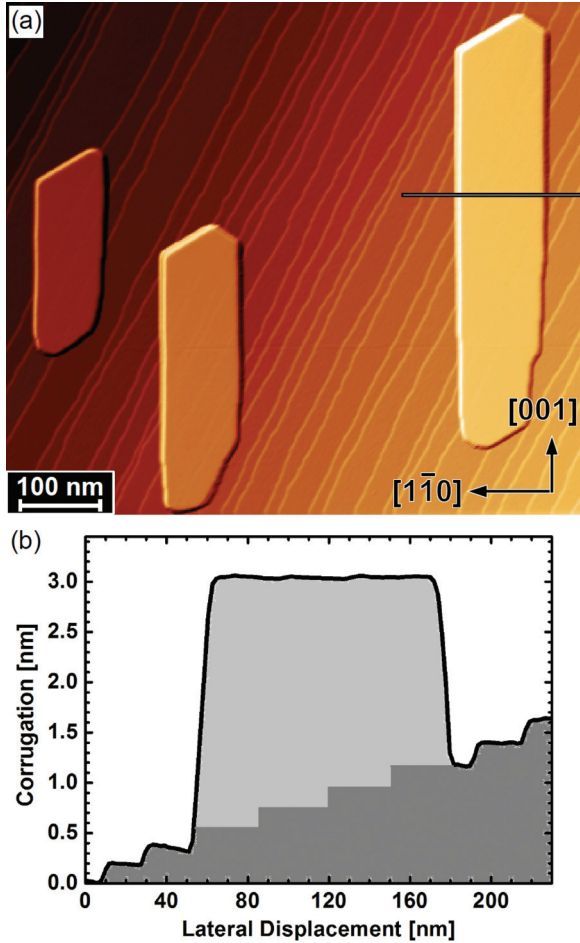
FIG. 1. (Color online) (a) STM image of Cr islands grown on W(110). Scan parameters are $U = 1.0$ V, $I = 30$ pA. (b) Line profile taken along the black line across the right island in panel (a).

at 650 K. The Cr islands exhibit an elongated shape with the long axis along the [001] direction. As indicated by the line profile taken along the line in Fig. 1(a), the surface of the Cr islands are atomically flat [Fig. 1(b)]. Since each Cr island covers numerous step edges of the underlying W(110) substrate, the local coverage varies significantly across the island area. In this particular case, with substrate terraces descending from the lower right to the upper left corner of the image, the thickness of Cr islands in Fig. 1(a) decreases from top to the bottom. Thereby, in close analogy to so-called wedge experiments performed on macroscopic films,[32,33] these islands can be viewed as nanowedges. In contrast to the previous works where wedges were probed with synchrotron radiation with spot sizes in the range of 100 μm, the high spatial resolution of scanning tunneling microscopy allows us to investigate the local structural, electronic, and magnetic properties down to the atomic scale.

An island with a relatively low local Cr thickness ranging from 0.8 ± 0.1 nm in the lower right corner up to 1.4 ± 0.1 nm close to the upper left edge is shown in Fig. 2(a). Clearly, a periodic corrugation called a moiré pattern can be recognized on the surface of the island. The formation of the moiré pattern is attributed to the lattice mismatch between the Cr island and the W substrate. While both materials crystallize

in the bcc structure, the bulk lattice constant of Cr is about 9% smaller than that of W. Furthermore, the lattice-constant difference also leads to a slight difference of the atomic layer thickness between Cr and W. In other words, the buried W step edges cause small steps on the surface of the Cr islands.[34] For example, the two arrows in Fig. 2(a) indicate the position of a W step edge underneath the surface. At this position the intensity of the moiré pattern reduces as the thickness of Cr island increases.

Figures 2(b) and 2(c) show zoomed-in STM images of the moiré pattern observed on a different Cr island. The local thicknesses are 0.6 ± 0.1 nm and 2.6 ± 0.1 nm, respectively. To measure the lateral periodicity of the moiré pattern quantitatively, we performed a one-dimensional Fourier transform (1D-FFT) along the [1$\bar{1}$0] and the [001] direction, as shown in Figs. 2(d), 2(e), 2(f), and 2(g), respectively. The corresponding line profiles taken along the hatched lines across the 1D-FFT pattern are shown in Figs. 2(h) and 2(i). The corrugation of the moiré pattern drastically decreases with increasing Cr thickness as indicated by the strong reduction in the 1D-FFT peak intensity. Detailed analysis reveals that, as the local Cr thickness increases from 0.6 ± 0.1 nm to 2.6 ± 0.1 nm, the periodicity of surface moiré pattern reduces by about 17% along the [1$\bar{1}$0] direction and by 12% for the [001] direction.

The periodicities of the moiré patterns acquired from STM images allows for an estimation of the surface strain of the Cr island.[34,35] The periodicity of the moiré structure along the [1$\bar{1}$0] direction is given by

$$\frac{2\pi}{l_{[1\bar{1}0]}} = \left| \frac{2\pi}{a_{\mathrm{Cr}[1\bar{1}0]}} - \frac{2\pi}{a_{\mathrm{W}[1\bar{1}0]}} \right|, \tag{1}$$

where $l_{[1\bar{1}0]}$ is the periodicity of the moiré structure along the [1$\bar{1}$0] direction, and $a_{\mathrm{Cr}[1\bar{1}0]}$ and $a_{\mathrm{W}[1\bar{1}0]}$ are the bulk lattice constants of Cr and W, respectively. Defining strain as $\epsilon_{[1\bar{1}0]} = \Delta a / a$, we obtain $\epsilon_{[1\bar{1}0]} \approx 0.6\%$ and $\epsilon_{[001]} \approx 0.3\%$ for Cr at a thickness of 2.6 ± 0.1 nm. This means that the large misfit of about 9% between the lattice constants of Cr and W is largely relaxed at the surface of islands with a thickness of a few nanometers.

At Cr coverages beyond about 4 nm the corrugation of the moiré pattern in constant-current images disappears or becomes so tiny that it drops below the noise level of our STM, which amounts to about 2 pm. At the same time the CDW emerges on the top surface of the Cr island. Figure 3(a) shows a Cr island with lateral dimensions of about 150 nm by 500 nm along the [1$\bar{1}$0] and the [001] directions, respectively. As usual, this island covers numerous step edges of the W substrate but is atomically flat on top. Therefore, its local thickness ranges from 3.1 ± 0.2 nm at the bottom part of the image to 5.2 ± 0.2 nm in the upper part. Zooming in to the atomically flat island surface [Fig. 3(b)], there are 12 diagonal stripes with a typical separation of about 20–40 nm. These stripes are caused by buried W step edges in aforementioned text.

Interestingly, faint periodic dark stripes running along the [001] direction (long side of the image) appear with large corrugation at bias voltages below 150 mV. Similar to earlier STM observation on the Cr(110) surface of a monocrystalline sample,[15] these stripes are identified as wavefronts of the CDW
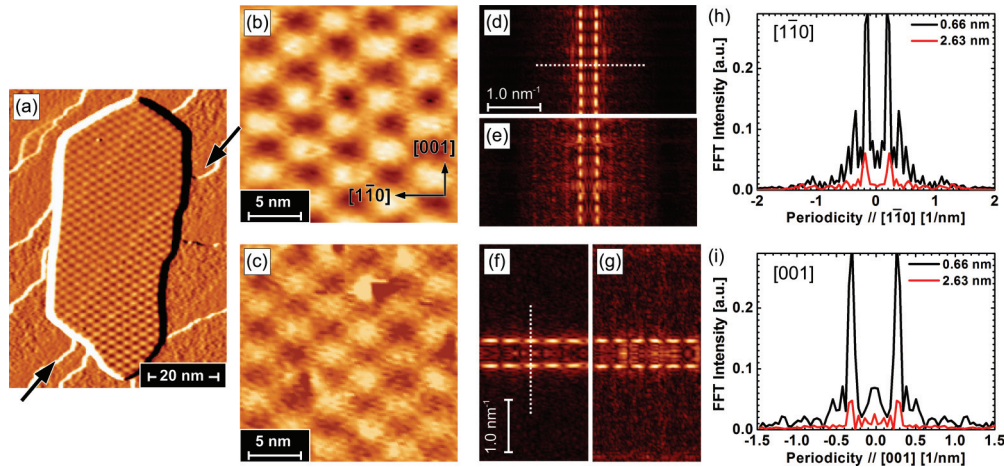
FIG. 2. (Color online) (a) Derivative (dz/dx) map of a topographic STM image showing the moiré pattern on top of a Cr island (scan parameters: $U = 1.0$ V, $I = 30$ pA). High-resolution images of the moiré pattern measured at local island thicknesses of (b) $\Theta_{loc} = 0.66$ nm and (c) $\Theta_{loc} = 2.63$ nm. These images were analyzed by taking 1D-FFT along the [(d) and (e)] perpendicular and the [(f) and (g)] horizontal direction. Panels (h) and (i) show line sections taken along the [1$\bar{1}$0] and along the [001] direction, respectively.

phase. In agreement with Ref. 15 we also find a periodicity of 5.95 ± 0.35 nm on thin islands, which is larger by a factor of
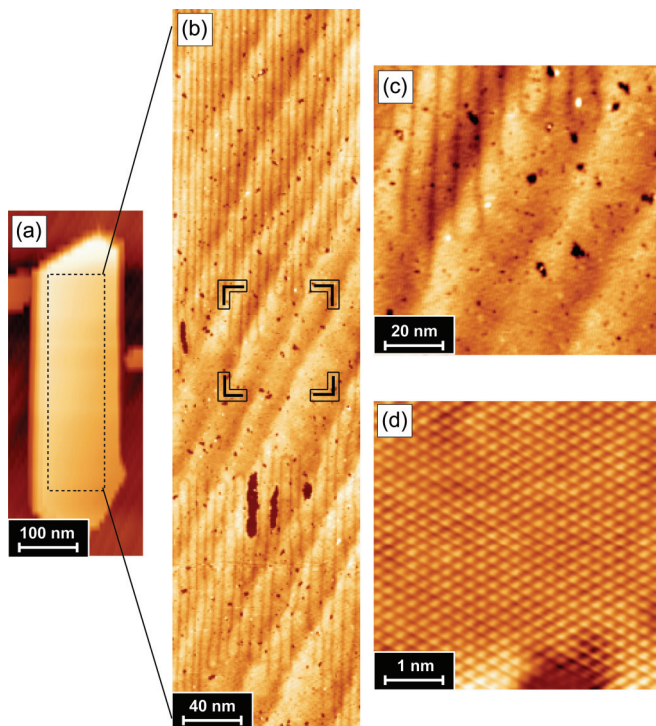

FIG. 3. (Color online) (a) Overall morphology of a large Cr island at 50 K. (b) Higher-magnification image of the island surface. Clearly, periodic stripes running along the [001] direction are present in the upper and the lower part of the image, corresponding to a CDW propagating in the [1$\bar{1}$0] direction. However, the CDW is absent in the central part (called the CDW gap. Scan parameters are $U = 1.0$ V, $I = 30$ pA. (c) Zoomed-in image taken inside the rectangle indicated in Panel (b). While some dark stripes are truncated, some strips connect to each others. (d) Topography with atomic resolution taken inside the CDW gap region. Scan parameters are $U = 10$ mV, $I = 1$ nA.
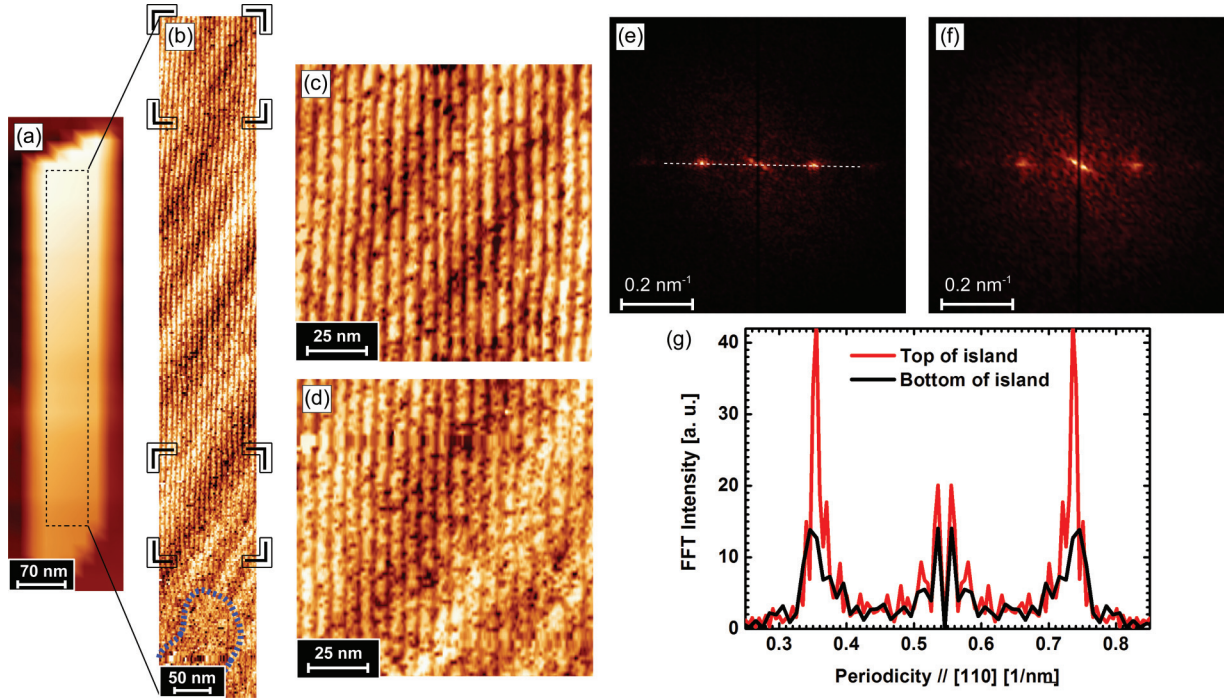
$\sqrt{2}$ than the bulk value ($\sim$4.2 nm). Even though our results are in general agreement with the voltage-dependent corrugation studies of Ref. 15 which demonstrated that the corrugation decreases with increasing bias voltage, our experiments reveal that the CDW is even visible at relatively high sample-bias voltages of about 1 V [cf. Fig. 3(b)]. Furthermore, we find some important differences between the (110) surface of a Cr crystal and that of nanoscale Cr islands on a W(110) surface: (i) In addition to the majority of CDW domains with wave vectors **Q** along the [100] or the [010] direction, which are tilted by 45° with respect to the surface, Braun *et al.* observed a few domains with **Q** along the [001] direction; i.e., within the surface plane.[15] The **Q** $\parallel$ [001] domains are characterized by wavefronts along the [1$\bar{1}$0] direction. We did not find this kind of domains on the Cr nanoislands studied in this work. (ii) While the wavefronts of the CDW are clearly observed in the lower and the upper part of the image, there is a region roughly in the middle of Fig. 3(b) where the CDW vanishes. This region is hereinafter called CDW gap.

We examined numerous islands with CDW gap regions which always appeared at film thicknesses around 4.5 nm. If the film thickness were the dominant control parameter that influence the SDW formation, the CDW gap would follow the the W(110) substrate step edges. Since this is not the case, other factors such as island geometry and substrate step-edge orientation must also play important roles. In order to have a closer look at the CDW gap region, a zoomed-in STM image of the upper boundary of the CDW gap region is shown in Fig. 3(c). Interestingly, some of the CDW wavefronts form connected pairs at the boundary, while others appear truncated. Figure 3(d) shows an atomic-resolution image taken inside the CDW gap region. We do not find any indications of the CDW corrugation but only an atomic-scale corrugation that is consistent with the (110) surface of a bcc crystal.

At this point it is important to recall that in the case of bulk Cr the CDW and the SDW are closely connected. Existing experimental data strongly suggest that the the incommensurate SDW ground state is a result of the nesting of certain Fermi wave vectors which then—by means of the spin-orbit

FIG. 4. (Color online) (a) Morphology of Cr island with thickness varying from $\Theta_{loc} = (3.6 \pm 0.2)$ nm in the lower part up to $\Theta_{loc} = (8.0 \pm 0.2)$ nm in the upper part. Scan parameters are $U = 1.0$ V, $I = 30$ pA. (b) Image taken on top of the island shown in panel (a) showing the wavefronts of the CDW and the CDW gap at the bottom (see area surrounded by a hatched line), Scan parameters are $U = 20$ mV, $I = 100$ pA. [(c) and (d)] High-resolution images taken within the framed boxes at the top and the bottom of panel (b), respectively. [(e) and (f)] Corresponding FFT analysis. (g) Comparison of line profiles reveals that the CDW wavelength increases for thinner Cr island.

interaction—gives rise to the CDW.[4,12,15] Consequently, the disappearance of CDW modulation in the gap region implies that the magnetic properties of Cr islands are quite different from that of Cr bulk crystals.

To quantify the thickness dependence of the CDW periodicity on Cr(110) islands, we have performed a detailed analysis of the CDW pattern observed on numerous long islands. One such example is shown in Fig. 4. The thickness of this island ranges from 3.6 ± 0.2 nm (lower part) to 8.0 ± 0.2 nm (upper part). As shown in Fig. 4(b), the CDW gap appears in the region surrounded by a dashed curve at the bottom of Fig. 4(a). Figures 4(c) and 4(d) show higher magnification images [taken within the two framed areas in Fig. 4(b)] of the CDW modulations at the low and high thickness, respectively. The corresponding FFT analysis [Figs. 4(e) and 4(f)] reveals a pair of pronounced spots at wave vectors equivalent to the inverse periodicity of the CDW modulation. From the line profiles taken in the FFT maps illustrated in Fig. 4(g), we obtained 5.23 ± 0.13 nm and 4.96 ± 0.15 nm for films thicknesses of 3.7 ± 0.2 nm and 7.3 ± 0.2 nm, respectively. Note that a similar thickness dependence of the CDW periodicity was reported in earlier studies of macroscopically wedged Cr(110) thin films grown on the W(110),[32] where the SDW periodicity was extracted from the weakly back-folded band structure measured with angle-resolved photoelectron emission spectroscopy (ARPES). However, the reported periodicity variation in previous studies[32] was much stronger than the one observed here by means of STM.

Figure 5(a) shows the thickness dependence of periodicities of the moiré pattern (red and blue symbols) and of the
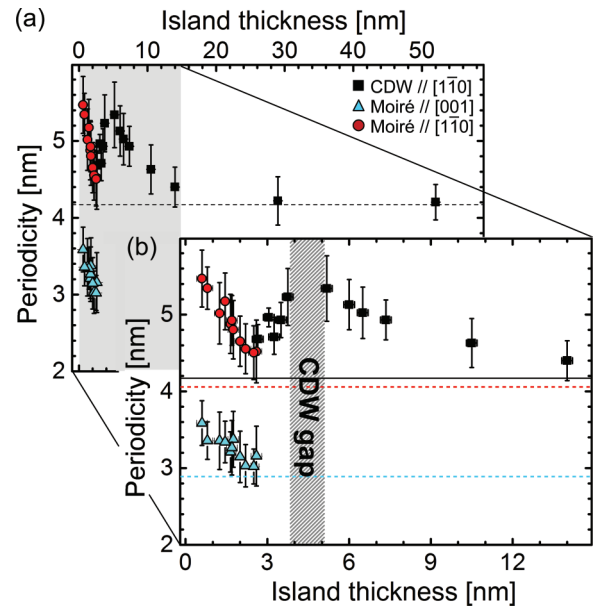

FIG. 5. (Color online) (a) Thickness-dependent CDW wavelength (black squares) and moiré periodicity along the [001] (blue triangles) and [1$\bar{1}$0] directions (red circles), respectively. The black dashed line indicates the bulk value of CDW periodicity along the [1$\bar{1}$0] direction ($\lambda_{CDW} \approx 4.2$ nm). (b) Zoomed-in image of panel (a) to show the CDW gap region. Red and blue dashed lines are the moiré periodicities expected for Cr bulk lattice constants $a_{[001]} \approx 2.88$ Å and $a_{[1\bar{1}0]} \approx 4.07$ Å, respectively.

CDW (black symbols) obtained from numerous Cr nanoislands. With the exception of a very narrow thickness range (2.5 nm < Θ < 5 nm), the periodicity of both the moiré pattern and the CDW decreases with increasing film thickness. A zoomed-in graph is shown in Fig. 5(b). It reveals that the CDW periodicity increases with thickness within a narrow band of local island thickness ranging from $\Theta = 2.5$ up to $\Theta = 3.7$ nm. Furthermore, no CDW modulation is found in the CDW gap region (3.7 nm < Θ_{gap} < 5.3 nm). The existence of the CDW gap in Fig. 5(b) demonstrates that nanoscale Cr islands possess fundamentally different magnetic properties than bulk Cr.

In order to understand the magnetic structure of the islands' surface we performed SP-STM measurements at the boundary of the CDW gap region. Magnetically coated tips were first characterized on the Mn monolayer on W(110). It is known that this sample exhibits an antiferromagnetic cycloidal spin structure where the local magnetization axis alternates between out-of-plane and in-plane with a period of about 6 nm.[29–31] As a result of the spin-orbit interaction (SOI) this magnetic structure is accompanied by a periodic variation of the spin-averaged local density of states (LDOS).[36] Within this so-called spin-orbit contrast (SOC) a high (low) LDOS corresponds to magnetic moments oriented in plane (out of plane). The upper

panel of Fig. 6(a) shows a SP-STM image of the Mn monolayer on W(110) measured with an Fe-coated probe tip which is expected to be sensitive to the in-plane spin component. In addition to the long-wavelength modulation, i.e., the SOC caused by the SOI, we observed an atomic-scale corrugation due to the spin-polarized contribution to the tunneling current. In fact, maximal spin-polarized contrast coincides with the maximum of the SOC [see line section in lower panel of Fig. 6(a)], thereby confirming the in-plane sensitivity of the Fe-coated tip.

After being characterized on Mn/W(110), the same in-plane sensitive tip was used to resolve the spin structures around the boundary between the CDW and the CDW gap area on a Cr nanoislands. While the topography (not shown here) is dominated by the CDW, the differentiated constant-current SP-STM image of Fig. 6(b) clearly shows the coexistence of a long- and a short-wavelength modulation in the upper part of the image. The long-wavelength modulation exhibits a periodicity of about 5.5 nm and is caused by the CDW. The faint modulation at shorter wavelength has a periodicity of ≈0.41 nm, i.e., about twice the atomic-row spacing along the [1$\bar{1}$0] direction. This observation is inconsistent with a (spin-averaged) surface atomic corrugation but agrees well with the magnetic doubling of the periodicity expected for a spin-resolved measurement of the row-wise antiferromagnetic Cr(110) surface.

In fact, the Fourier-transformed data shown in the inset of Fig. 6(c) reveal a pair of satellites caused by the incommensurability of the SDW. Such satellites were only observed in spin-polarized measurements; no indication was ever found in any measurements performed with bare W tips.[16] The periodicities extracted from the FFT line profiles correspond to about 12–13 and 24–26 lattice constants for the CDW and SDW, respectively. Due to the pronounced thickness dependence of the CDW/SDW periodicity in Cr(110) islands (cf. Fig. 5), these values are slightly larger than in the case of Cr(110) films reported before.[16,37]

In order to analyze the correlation of the CDW and the SDW at the boundary of the CDW in detail, we chopped the SP-STM image of Fig. 6(b) into 2-nm-wide segments (indicated by white lines). The averaged line profile of each segment was then analyzed by FFT. Figure 6(d) shows a plot of the peak intensities associated with the CDW (red data points) and the SDW (black). Obviously, the FFT peak intensity characteristic for the SDW drops simultaneously with the CDW peak intensity, indicating the close correlation of the CDW and the SDW.

A similar data set but now obtained with a Ni tip is shown in Fig. 7. In this case the characterization measurement shows a significant magnetic contrast at the minimum of the SOC of the Mn monolayer on W(110) [Fig. 7(a)], thereby indicating a substantial out-of-plane component to the Ni-tip magnetization. Again, with a magnetic probe tip both the CDW and the SDW modulation can be observed in the right part of the image but no magnetic contrast is obtained within the CDW gap (left side of the image).

The measurements performed with in-plane- and out-of-plane-sensitive tips which were presented in Figs. 6 and 7, respectively, indicate a canted surface magnetization of Cr(110) within the CDW/SDW area. Furthermore, irrespective of the tip-magnetization direction no magnetic contrast was
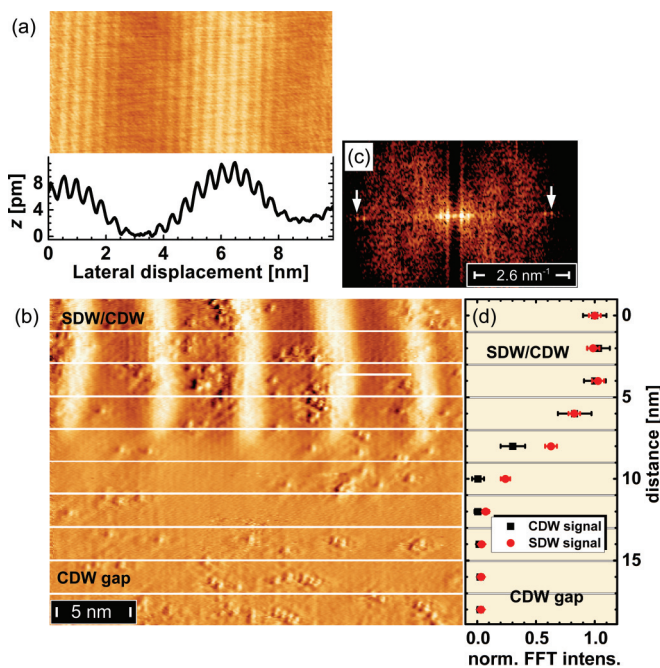
FIG. 6. (Color online) (a) Tip characterization of an Fe-coated probe tip (scan parameters are $U = 150$ mV, $I = 1$ nA) on a Mn monolayer on W(110) which exhibits a cycloidal AFM spin structure. As revealed by the line section (lower panel), the row-wise magnetic corrugation coincides with the maximum of the spin-orbit contrast (SOC) (periodicity 6 nm), indicating in-plane sensitivity. (b) Differentiated constant-current image image (dz/dx) of the boundary region of the CDW gap. measured with the same in-plane-sensitive tip characterized in panel (a) ($U = 10$ mV, $I = 6$ nA). (c) FFT-transform of panel (b) showing the pair of satellites characteristic for the SDW. (d) Plot of the FFT intensity associated with the CDW (red data points) and the SDW (black) as measured within the corresponding segments in panel (b).
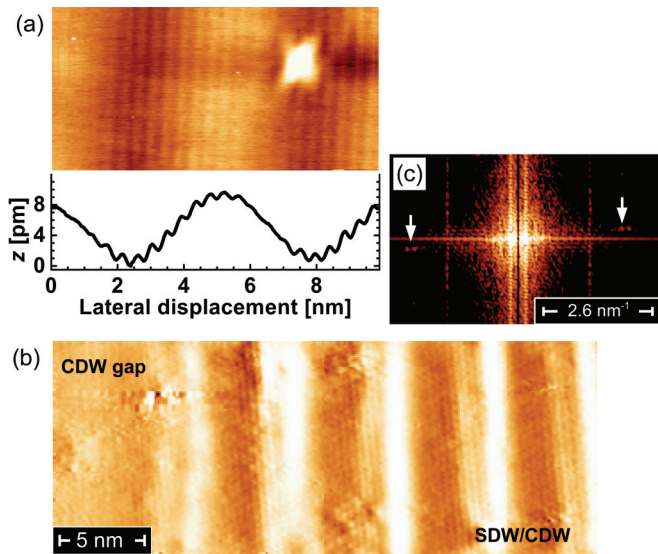
FIG. 7. (Color online) (a) SP-STM measurement on 1 AL Mn/W(110) performed with Ni tip. Maximum magnetic contrast is observed near the minimum of the SOC, indicating out-of-plane sensitivity ($U = 8$ mV, $I = 5$ nA). (b) Differentiated constant-current image image (dz/dx) of the boundary region of the CDW gap measured with the same out-of-plane-sensitive tip characterized in panel (a) ($U = 10$ mV, $I = 6$ nA). (c) FFT-transform of panel (b) showing the pair of satellites characteristic for the SDW.

observed within the CDW gap. Therefore, our experimental observation of a vanishing CDW signal at the island surface within a certain thickness range can, in principle, be explained by two scenarios: (i) Cr grown on W(110) within the CDW gap is nonmagnetic or (ii) the strain within the island modifies the SDW such that it exhibits a the node at the surface of the island. In case (i) the nonmagnetic state would represent the equilibrium state of Cr/W(110), i.e., the CDW gap region would become wider as the temperature is decreased. In contrast, if epitaxial strain locally forces the CDW to pin with the node at the islands surface [case (ii)], thermal fluctuations are expected to soften the boundary conditions, resulting in a gap region which becomes narrower at lower temperature.

Figure 8(a) shows a STM image taken at $T = 48$ K. While the CDW can clearly be recognized in the left part of the image its absence in the right indicates the presence of the CDW gap. After changing the sample temperature to $T = 106$ K the same location of the sample was imaged again. Comparison of Figs. 8(a) and 8(b) reveals that the CDW withdraws and the gap region becomes wider at higher temperature. Details such as the remaining closed-loop structure of the CDW in Fig. 8(b) (see arrow) indicate that intriguing spin rearrangement processes must have occurred during the temperature change. Surprisingly, this process is reversible and the CDW region recovered its original configuration when the sample was cooled down again [see Fig. 8(c) taken at $T = 51$ K]. No further variation was observed when lowering the temperature down to the $T = 35$ K [see Fig. 8(d)]. These results indicate that the scenario of a nonmagnetic phase of Cr in the CDW gap region can likely be excluded. Instead, we believe that the appearance of a SDW gap has to be interpreted in terms of a SDW wave which is pinned with a node at the island surface.

While STM can provide detailed information on structural and electronic properties of surfaces, its high surface sensitivity prevents us from looking into the bulk of the sample. Therefore, we can only speculate how the spin structure, which results in the CDW surface gap and the significant increase of the CDW wavelength at Cr film thicknesses around the CDW gap, might look like within the island. In the following text we present two models of the spin structure to explain our experimental observations.

As shown in Fig. 9(a), the surface SDW/CDW gap region could be explained by a SDW with wave vector **Q** normal to the (110) surface. The spin structure can be viewed as a superposition of a transverse and a longitudinal SDW propagating along the blue and red lines, respectively, as illustrated in Fig. 9(a). Note that **Q** ∥ [110] has never been observed in bulk Cr. The spin model in Fig. 9(b) indicates a reorientation transition of the wave vector; for example, from the [100] direction via the [110] direction into the [010] direction as the island thickness varies. In bulk Cr crystals, the SDW **Q** is along the ⟨001⟩ axes due to Fermi surface nesting.[4,12,15] In the thick-film limit [right part of Fig. 9(b)] the SDW **Q** propagates along one of the ⟨001⟩-type direction which is
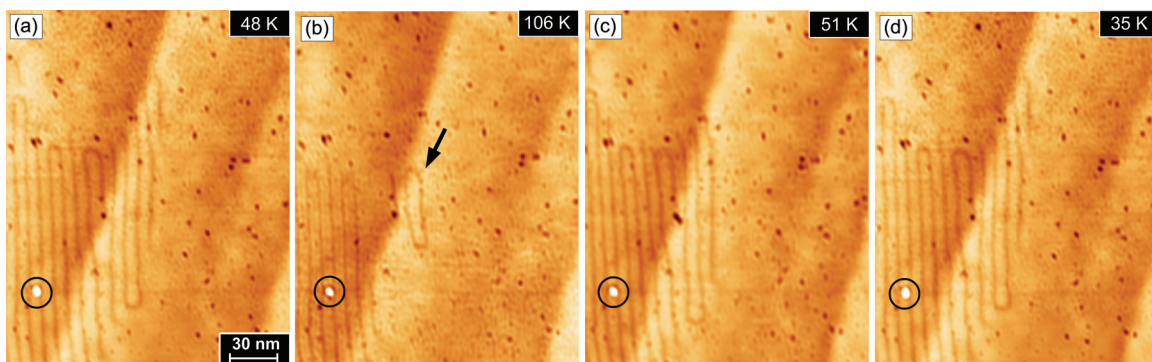

FIG. 8. (Color online) STM images taken at various temperatures show the evolution in the proximity between the CDW and the CDW gap (scan parameters: $U = 1$ V, $I = 150$ pA). Black circles mark the same impurity in different images. The CDW gap broadens as the temperature is increased from (a) $T = 48$ K to (b) $T = 106$ K. In addition, the CDW rearranges and occasionally forms closed loops (arrow). (c) Cooling the sample back down to 51 K almost recovers the surface distribution of the CDW and the CDW gap. (d) Further cooling to $T = 35$ K has little effect on the CDW.
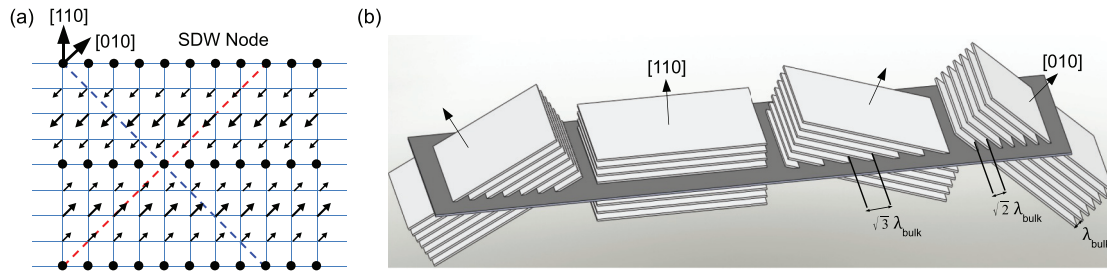
FIG. 9. (Color online) Models of SDW in Cr(110) islands. (a) Cartoon of spin structure of SDW with node at the Cr(110) surface at SDW gap region. (b) Model of apparent thickness dependence of SDW wavelength by reorientation transition of SDW (see text for details).

tilted 45° relative to the surface normal, resulting in an apparent CDW modulation wavelength $\lambda_{surf} = \sqrt{2}\lambda_{bulk} \approx 4.2$ nm.[16] As the island thickness decreases, **Q** gradually rotates toward the other ⟨100⟩-type direction, resulting in a gradual increase of the wavelength of the surface-projected CDW. However, too much deviation from the preferred nesting wave vector would likely destabilize the SDW, forming a SDW node region in the middle of **Q** rotation. As the film thickness is further reduced, the SDW wave vector tilts back toward the ⟨001⟩ directions [left part of Fig. 9(b)] so that the projected CDW modulation gradually decreases.

The reorientation transition and surface pinning might be caused by surface and interface contributions to the total energy, which are known to play important roles in the magnetic properties in thin Cr films.[37,38] For example, thickness-dependent CDW periodicities have also been observed in the thin Cr(110) films grown on W(110).[32,33] While they found little to no changes in the Fermi-surface nesting vector, Rotenberg *et al.* report on the thickness-dependent transition from an incommensurate SDW in the thick-film limit (12 nm) to a commensurate SDW for films of around 3 nm. This transition is accompanied by a three-fold increase in SDW wavelength, which was interpreted as a reorientation of the SDW wave vector from perpendicular to the film plane to in plane.[32,33] However, we did not observe any $c(2 \times 2)$ surface spin structure characteristic for the commensurate SDW by SP-STM within the CDW gap. Therefore, we can strictly rule out this scenario for Cr(110) islands grown on W(110). Instead, our results indicate that the SDW pins with a node at the surface. Similar pinning effects, although with an antinode pinned at the surface, have been observed for the Cr(001) surface which presents the layered antiferromagnetic surface spin structures.[39,40]

IV. SUMMARY

In summary, we have determined the surface strain of Cr islands grown on W(110) by analyzing the surface moiré pattern. We find that the periodicity of the CDW increases by about 30% with respect to the bulk value when decreasing the film thickness Θ down to about 5.2 nm. At film thicknesses $3.7 \leqslant \Theta \leqslant 5.2$ nm we observe a so-called CDW gap where the CDW vanishes. By employing out-of-plane- and in-plane-sensitive tips we show by SP-STM that the Cr(110) island surface is nonmagnetic within the CDW gap. At film thicknesses $2.5 \leqslant \Theta \leqslant 3.7$ nm the CDW reappears, before it vanishes at even lower coverages. We present a model that explains the thickness dependence of the SDW wavelength by a continuous rotation of the SDW vector **Q** from bulk-like ⟨001⟩ directions into the surface-normal [110] direction. The vanishing surface magnetic moment within the gap region is interpreted as a pinning of the SDW node at the island surface.

[1] J. R. Ahn, H. W. Yeom, H. S. Yoon, and I. W. Lyo, Phys. Rev. Lett. **91**, 196403 (2003).

[2] J. N. Crain and D. T. Pierce, Science **307**, 703 (2005).

[3] C. Blumenstein, J. Schäfer, S. Mietke, S. Meyer, A. Dollinger, M. Lochner, X. Y. Cui, L. Patthey, R. Matzdorf, and R. Claessen, Nat. Phys. **7**, 776 (2011).

[4] G. Grüner, Rev. Mod. Phys. **37**, 7673 (1988).

[5] B. Giambattista, A. Johnson, R. V. Coleman, B. Drake, and P. K. Hansma, Phys. Rev. B **37**, 2741 (1988).

[6] X. L. Wu and C. M. Lieber, Science **243**, 1703 (1989).

[7] J. M. Carpinelli, H. H. Weitering, E. W. Plummer, and R. Stumpf, Nature (London) **381**, 398 (1996).

[8] V. B. Zabolotnyy, D. S. Inosov, D. V. Evtushinsky, A. Koitzsch, A. A. Kordyuk, G. L. Sun, J. T. Park, D. Haug, V. Hinkov, A. V. Boris, C. T. Lin, M. Knupfer, A. N. Yaresko, B. Büchner, A. Varykhalov, R. Follath, S. V. Borisenko, and N. C. Koon, Nature (London) **457**, 569 (2009).

[9] M. Yi, D. H. Lu, J. G. Analytis, J.-H. Chu, S.-K. Mo, R.-H. He, M. Hashimoto, R. G. Moore, I. I. Mazin, D. J. Singh, Z. Hussain, I. R. Fisher, and Z.-X. Shen, Phys. Rev. B **80**, 174510 (2009).

[10] J. Paglione and R. L. Greene, Nat. Phys. **6**, 645 (2010).

[11] P. C. Dai, J. P. Hu, and E. Dagotto, Nat. Phys. **8**, 709 (2012).

[12] E. Faucett, Rev. Mod. Phys. **60**, 209 (1988).

[13] M. N. Baibich, J. M. Broto, A. Fert, F. Nguyen Van Dau, F. Petroff, P. Etienne, G. Creuzet, A. Friederich, and J. Chazelas, Phys. Rev. Lett. **61**, 2472 (1988).

[14] G. Binasch, P. Grünberg, F. Saurenbach, and W. Zinn, Phys. Rev. B **39**, 4828 (1989).

[15] K. F. Braun, S. Folsch, G. Meyer, and K. H. Rieder, Phys. Rev. Lett. **85**, 3500 (2000).

[16] B. Santos, J. M. Puerta, J. I. Cerda, R. Stumpf, K. von Bergmann, R. Wiesendanger, M. Bode, K. F. McCarty, and J. de la Figuera, New J. Phys. **10**, 013005 (2008).

[17] M. Bode, S. Krause, L. Berbil-Bautista, S. Heinze, and R. Wiesendanger, Surf. Sci. **601**, 3308 (2007).

[18] A. Wachowiak, J. Wiebe, M. Bode, O. Pietzsch, M. Morgenstern, and R. Wiesendanger, Science **298**, 577 (2002).

[19] M. Bode, A. Wachowiak, J. Wiebe, A. Kubetzka, M. Morgenstern, and R. Wiesendanger, Appl. Phys. Lett. **84**, 948 (2004).

[20] W. Wulfhekel and J. Kirschner, Appl. Phys. Lett. **75**, 1944 (1999).

[21] M. Bode, Rep. Prog. Phys. **66**, 523 (2003).

[22] R. Wiesendanger, Rev. Mod. Phys. **81**, 1495 (2009).

[23] M. Bode, M. Getzlaff, and R. Wiesendanger, Phys. Rev. Lett. **81**, 4256 (1998).

[24] U. Schlickum, W. Wulfhekel, and J. Kirschner, Appl. Phys. Lett. **83**, 2016 (2003).

[25] C. B. Wu, P. J. Hsu, H. Y. Yen, and Minn-Tsong Lin, Appl. Phys. Lett. **91**, 202507 (2007).

[26] A. Kubetzka, M. Bode, O. Pietzsch, and R. Wiesendanger, Phys. Rev. Lett. **88**, 057201 (2002).

[27] H. F. Ding, W. Wulfhekel, J. Henk, P. Bruno, and J. Kirschner, Phys. Rev. Lett. **90**, 116603 (2003).

[28] P. J. Hsu, C. I. Lu, S. W. Chen, W. J. Hsueh, Y. H. Chu, C. H. Hsu, C. J. Butler, and M.-T. Lin, Appl. Phys. Lett. **96**, 142515 (2010).

[29] M. Bode, M. Heide, K. von Bergmann, P. Ferriani, S. Heinze, G. Bihlmayer, A. Kubetzka, O. Pietzsch, S. Blügel, and R. Wiesendanger, Nature (London) **447**, 190 (2007).

[30] P. Sessi, N. P. Guisinger, J. R. Guest, and M. Bode, Phys. Rev. Lett. **103**, 167201 (2009).

[31] D. Serrate, P. Ferriani, Y. Yoshida, S.-W. Hla, M. Menzel, K. von Bergmann, S. Heinze, A. Kubetzka, and R. Wiesendanger, Nat. Nanotechnol. **5**, 350 (2010).

[32] E. Rotenberg, B. K. Freelon, H. Koh, A. Bostwick, K. Rossnagel, A. Schmid, and S. D. Kevan, New J. Phys. **7**, 114 (2005).

[33] E. Rotenberg, O. Krupin, and S. D. Kevan, New J. Phys. **10**, 023003 (2008).

[34] A. Cazacu, S. Murphy, and I. V. Shvets, Phys. Rev. B **73**, 045413 (2006).

[35] K. Kobayashi, Phys. Rev. B **53**, 11091 (1996).

[36] M. Bode, S. Heinze, A. Kubetzka, O. Pietzsch, X. Nie, G. Bihlmayer, S. Blügel, and R. Wiesendanger, Phys. Rev. Lett. **89**, 237205 (2002).

[37] H. Zabel, J. Phys.: Condens. Matter **11**, 9303 (1999).

[38] P. Bodeker, A. Hucht, A. Schreyer, J. Borchers, F. Guthoff, and H. Zabel, Phys. Rev. Lett. **81**, 914 (1998).

[39] M. Kleiber, M. Bode, R. Ravlić, and R. Wiesendanger, Phys. Rev. Lett. **85**, 4606 (2000).

[40] T. Hänke, S. Krause, L. Berbil-Bautista, M. Bode, R. Wiesendanger, V. Wagner, D. Lott, and A. Schreyer, Phys. Rev. B **71**, 184407 (2005).